RESEARCH ARTICLE

Key Points:
- Saturation properties of whistler waves are investigated in a plasma with two electron components
- The temperature anisotropy and plasma beta relation is shown to be consistent with linear theory only within a certain range of plasma beta
- The saturation amplitude of waves can be modeled using the initial linear growth rate

Correspondence to:
X. Tao,
xtao@ustc.edu.cn

Saturation Properties of Whistler Wave Instability in a Plasma With Two Electron Components

Yifan Wu[1,2] **, Xin Tao**[1,2] **, Quanming Lu**[1,2]**, and Shui Wang**[1,2]

[1]CAS Key Laboratory of Geospace Environment, Department of Geophysics and Planetary Sciences, University of Science and Technology of China, Hefei, China, [2]CAS Center for Excellence in Comparative Planetology, Hefei, China

Abstract Saturation properties of whistler wave instability driven by electron temperature anisotropy in a plasma with two electron components are investigated using particle-in-cell (PIC) simulations. Most of the previous self-consistent PIC simulations or quasi-linear theory used a single bi-Maxwellian distribution of electrons, which might apply to solar wind or magnetosheath. In the inner magnetosphere, however, there is frequently a cold and dense electron component, coexisting with a hot electron component. In this work, we investigate the relation between temperature anisotropy (A) and parallel plasma beta ($\beta_\parallel$) at saturation. Our results agree well with the previous conclusion obtained from linear theory in most cases. However, We show that the inverse relation breaks when $\beta_\parallel$ is larger than certain value $\beta_{\parallel,\mathrm{lim}}$, beyond which A increases with increasing $\beta_\parallel$. We also investigated the dependence of the saturation wave intensity on plasma beta and the initial linear growth rate and show that the saturation amplitude can be modeled as a function of the maximum initial linear growth rate even in a plasma with two electron components. Our results might be useful to couple the microscopic wave excitation process with macroscopic global energetic electron dynamics and to understand whistler wave excitation in the inner magnetosphere.

1. Introduction

Whistler mode waves are electromagnetic emissions with frequency (ω) between the lower hybrid resonance frequency (ω_{LHR}) and the electron cyclotron frequency (Ω_e). These waves are commonly observed in the magnetosphere and play important roles in accelerating and scattering energetic electrons, leading to the formation of the outer electron radiation belt (Horne et al., 2005; Reeves et al., 2013; Thorne et al., 2013) and diffuse and pulsating aurora (e.g., Nishimura et al., 2010; Thorne et al., 2010). In the inner magnetosphere, whistler mode waves are typically driven by electron temperature anisotropy and reaches saturation within several hundreds or thousands of electron cyclotron periods. For a dipole L shell value of 5, the typical gyroperiod of electrons is about 10^{-4} s; therefore, whistler instability saturates within less than a second. As a result, if we investigate plasma conditions with satellite observations, we will most probably see two kinds of state: the whistler mode saturation state, or a more relaxed state in which whistler waves cannot be generated at all. This suggests the existence of whistler instability upper bound and the importance of studying saturation properties of whistler mode waves.

The purpose of this work is to investigate two kinds of saturation properties of whistler mode waves suitable for plasma conditions in the inner magnetosphere. The first saturation property we focus on is the relation between electron temperature anisotropy (A) and parallel plasma beta ($\beta_\parallel$). Previous studies for a single bi-Maxwellian electron distribution have demonstrated that at saturation, A and $\beta_\parallel$ can be modeled as

$$A = \frac{S}{\beta_\parallel^\alpha} \tag{1}$$

Here S and α are two fitting constants. These studies use either linear theory (Gary & Wang, 1996), particle-in-cell (PIC) simulations (An et al., 2017; Gary & Wang, 1996), or quasi-linear analysis (Davidson et al., 1972; Kim et al., 2017; Tao et al., 2017). Observations show good agreement with theory (Gary et al., 2005; Yue et al., 2016). Based on the assumption of single hot electron component, results of these studies should be applicable to the solar wind or the magnetosheath. However, for the inner magnetosphere, there typically exists a dense cold electron population and a hot electron component. Therefore, how the presence of cold electrons modifies equation (1) requires further quantitative study.

Using linear analysis, Gary et al. (2012) extended their analysis to bi-Maxwellian plasma into situation where cold electrons exist and studied the effect of the number density percentage of cold electrons in detail. They still found that even if cold electrons are added, the inverse relation between A and $\beta_\parallel$ for hot electrons can still be described by equation (1). Besides, assuming a threshold maximum growth rate, $\gamma_{\max} = 0.001\Omega_e$, Gary et al. (2012) also found that fitting parameters (S and α) depend on the percentage of the cold electron number density as

$$S = 0.206 - 0.107\frac{n_c}{n} - 0.0326\left(\frac{n_c}{n}\right)^2, \tag{2}$$

$$\alpha = 0.574 + 0.178\frac{n_c}{n} - 0.198\left(\frac{n_c}{n}\right)^2 \tag{3}$$

for $0.0 \leq n_c/n \leq 0.95$. Similar linear analysis for two-component electrons with bi-Kappa distributions have been done by Xiao et al. (2006). It is clear that linear theory cannot predict the value of S or α without assuming a value of $\gamma_{\max}$. Therefore, one motivation of this study is to test the previous conclusions about the A–$\beta_\parallel$ relation from linear theory (Gary et al., 2012) using self-consistent PIC simulations.

The second saturation property we are going to study is the saturation amplitude of whistler waves and its dependence on the initial linear growth rate or $\beta_\parallel$ at saturation. This is practically important because such kind of dependence could potentially allow the incorporation of microscopic physical processes (wave saturation) into macroscopic global models such as Ring current Atmosphere interactions Model (Jordanova et al., 2010). For a single bi-Maxwellian electron distribution, Tao et al. (2017) demonstrated using quasi-linear theory that the saturation intensity could be modeled as a function of the maximum initial linear growth rate. Using PIC simulations, An et al. (2017) modeled the saturation wave amplitude as a function of plasma beta at saturation. Therefore, the other purpose of this work is to study whether the relations between the saturation wave amplitude and the initial linear growth rate or plasma beta at saturation still apply with the presence of a dense cold electron population, and how they are affected by the percentage of the cold electron population.

The remaining part of the paper is organized as follows. We briefly introduce our simulation method in section 2 and show the simulation results with only hot electron distributions as the benchmark case in section 3. The simulation results with the presence of a cold electron component are presented in section 4. Finally, we discuss and summarize our work in section 5.

2. Simulation Method

A one-dimensional particle simulation code, DAWN (Tao, 2014), is used to investigate saturation properties of whistler wave instability with a cold electron component. In this code, waves are assumed to be parallel propagating along the z direction, and the velocity is fully 3-D. We use a one-dimensional simulation code, because for the range of $\beta_\parallel$ investigated in this study, the linear growth rate peaks in the parallel direction (Gary et al., 2011). The cold electron component is modeled using fluid equations to save computation time, and hot electrons are simulated using PIC techniques. When needed, however, both components can be modeled using PIC methods in the DAWN code. Since our main purpose is to compare with previous linear kinetic theories for an infinite uniform plasma, periodic boundary conditions are used for both waves and particles. Ions are assumed to be fixed, because whistler wave frequency is much larger than ion cyclotron frequency.

For each simulation below, we choose the grid size to be $0.05c\Omega_e^{-1}$ and the time step to be $0.02\Omega_e^{-1}$ to satisfy the Courant condition ($\Delta z \geq c\Delta t$). Thus, for each period of whistler mode waves, at least 314 time steps are calculated. The system contains 1024 cells, and the full length is $51.2c\Omega_e^{-1}$, which is typically 10 times larger than the wave length of the most unstable mode. The number of time steps is chosen to be large enough so that the macroscopic properties of plasma such as wave amplitude and electron temperature do not change significantly at the final stage. For each cell, 500 super particles are used. These settings allow small enough sampling noise level to obtain the saturation properties of waves and plasmas in all cases below.

3. Results With Hot Electrons Only

As a benchmark case and the demonstration of our method, we first use simulation to find the A–$\beta_\parallel$ relation in a plasma with only a hot electron component and parallel propagating whistler waves. Such a case has
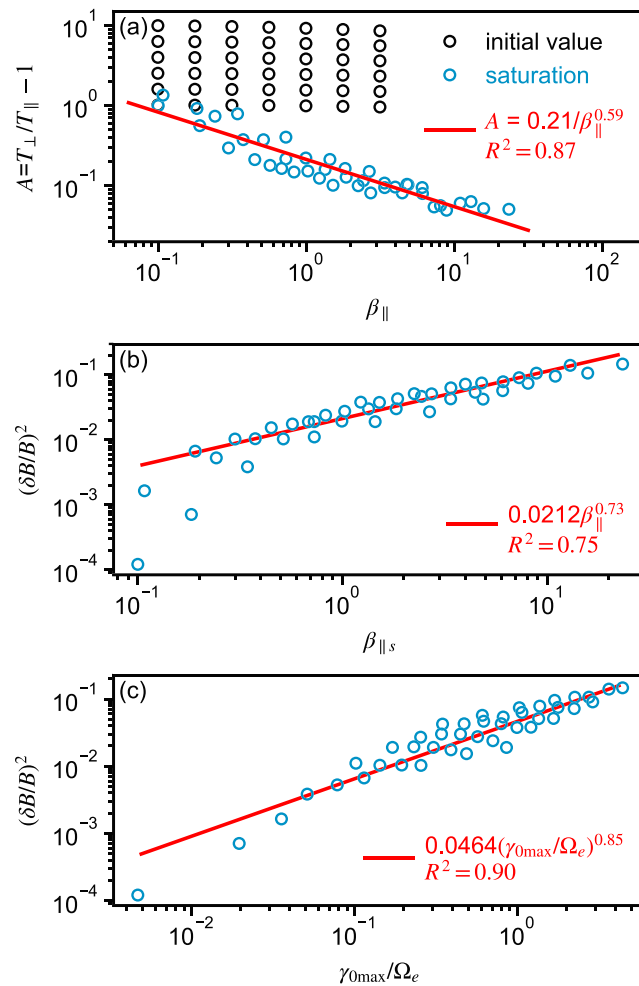
Figure 1. (a) Initial and saturated hot electron temperature anisotropy and parallel plasma beta. Black circles represent initial values, and blue for saturated. The red line shows the fitting result of $A = S/\beta_\parallel^\alpha$. (b) Saturated wave intensity (represented by average value of $(\delta B/B)^2$) and $\beta_\parallel$ (blue circles), and a least absolute deviation fitting (red line). (c) Saturated wave intensity and maximum initial linear growth rate γ_{max}, and least absolute deviation fitting results for them.

been well studied by several authors using different methods, including linear (Gary & Wang, 1996) and quasi-linear analysis (Tao et al., 2017), and PIC simulations (Gary & Wang, 1996).

To obtain the relation between the saturation temperature anisotropy and parallel plasma beta, we perform series of simulations using the DAWN code with different initial conditions (Figure 1). In this work, we select six different initial A's times seven different initial $\beta_\parallel$'s. The initial $\beta_\parallel$'s are logarithmically evenly spaced between 0.1 and 3, and the initial A's are logarithmically evenly spaced between 1 and 10, shown as black dots in Figure 1a. The plasma frequency ($\omega_{pe} \equiv \sqrt{4\pi n e^2/m}$) is chosen to be $\omega_{pe} = 4\Omega_e$, where $\Omega_e = eB/mc$ is the unsigned positive electron cyclotron frequency, n is the electron number density, B is the background magnetic field strength, e is the unit charge, m is the electron mass, and c is the speed of light in vacuum. In cases of whistler instability driven by temperature anisotropy, wave scattering leads to the decrease of the temperature anisotropy and the increase of parallel temperature, and therefore, the $\beta_\parallel$ becomes larger than its initial values. Consistent with previous studies, Figure 1a shows that the saturation A-$\beta_\parallel$ relation can be well fit by a straight line with a negative slope in a log-log plot, indicating that A and $\beta_\parallel$ can be described by the inverse power law function: $A = S/\beta_\parallel^\alpha$ with $S > 0$ and $\alpha > 0$. Linear fitting of $\log A$ and $\log \beta_\parallel$ results in $S = 0.213$ and $\alpha = 0.590$, which agree well with previous research by Gary and Wang (1996); Kim et al. (2017); Tao et al. (2017) using linear, PIC, or quasi-linear analysis.
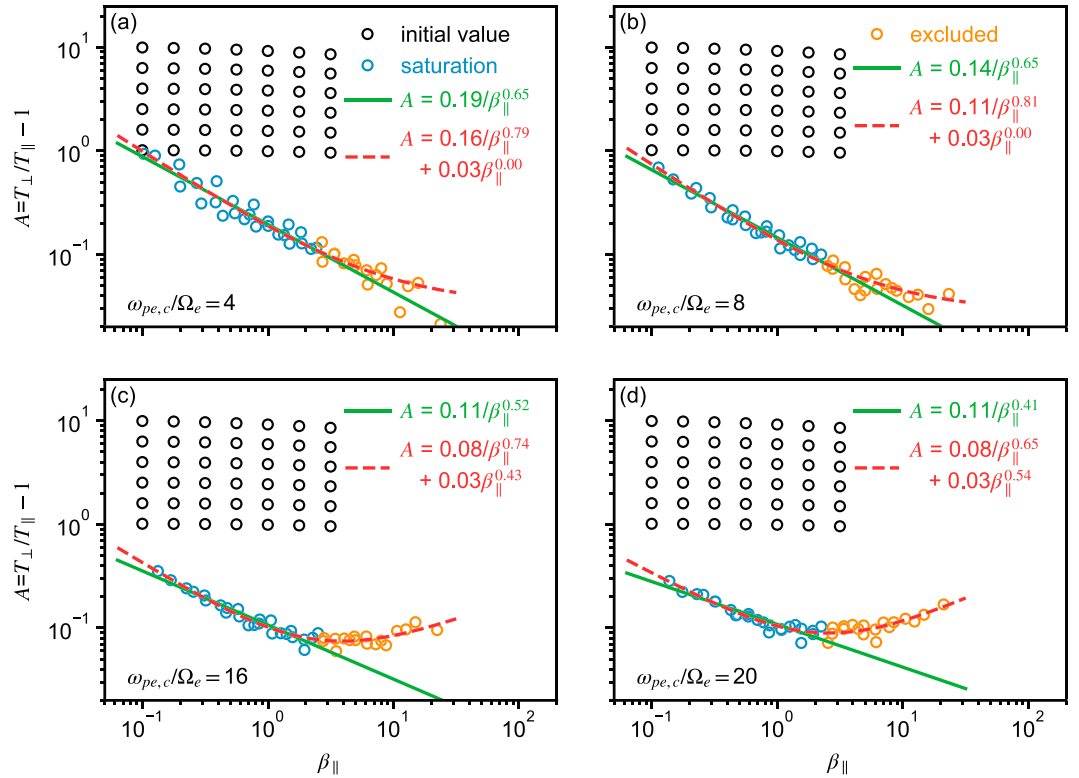
Figure 2. Saturated $A - \beta_\parallel$ for different cold electron density. $\omega_{pe,c}/\Omega_e = 4, 8, 16$ and 20 for (a), (b), (c), and (d), respectively. Black circles represent initial values while blue and orange circles mark the saturated value. Two kinds of fitting are shown in different colors. The solid green lines represent the first fitting method, in which only cases with $\beta_\parallel < 2.5$ are used (blue circles). Cases with $\beta_\parallel$ beyond this range are denoted as orange circles. The dashed red curves show fitting results of the new fitting function, for which both blue and orange circles are used.

Figures 1b and 1c present the saturation wave intensity, $(\delta B/B)^2$, as a function of $\beta_\parallel$ at saturation and the maximum initial linear growth rate, following previous studies of An et al. (2017) and Tao et al. (2017). The R^2 parameter, which is also called the coefficient of determination, for a fitting function $f(x)$ used for data x_i and y_i is defined as

$$R^2 = 1 - \frac{\sum_i (y_i - f_i)^2}{\sum_i (y_i - \langle y_i \rangle)^2}, \tag{4}$$

where x is the independent variable. The value of R^2 being close to 1 indicates that the fitting results are consistent with the input data. Comparing R^2 of Figures 1b and 1c, where R^2 is 0.75 and 0.90, respectively, we conclude that the saturation wave intensity can be better modeled as a function of the initial γ_{max} than $\beta_\parallel$ at saturation. This is also consistent with those of Tao et al. (2017).

4. Results With a Cold Electron Component

To investigate the effect of adding a cold electron component on saturation properties of whistler waves, we fix the plasma frequency of the hot electron component and vary the number density of the cold electron component, following Gary et al. (2012). We choose seven different cold electron number densities: $\omega_{pe,c}/\Omega_e = 2, 4, 6, 8, 12, 16$, and 20, or $\omega_{pe,c}/\omega_{pe,h} = 0.5, 1, 1.5, 2, 3, 4$, and 5 for $\omega_{pe,h}/\Omega_e = 4$, respectively. For $\omega_{pe,c}/\Omega_e = 20$, $n_c/n \approx 96\%$. Here subscript c denotes the cold electron component, h denotes the hot component, and n is the total number density. The range of the cold electron number density is roughly consistent with that of Gary et al. (2012).

4.1. Saturation Relation Between A and $\beta_\parallel$

We set up other initial parameters in the same way as in section 3. For each $\omega_{pe,c}$, we perform 42 simulations, six for A and seven for $\beta_\parallel$, to find saturation properties. Four characteristic results with $\omega_{pe,c}/\Omega_e = 4, 8, 16, 20$
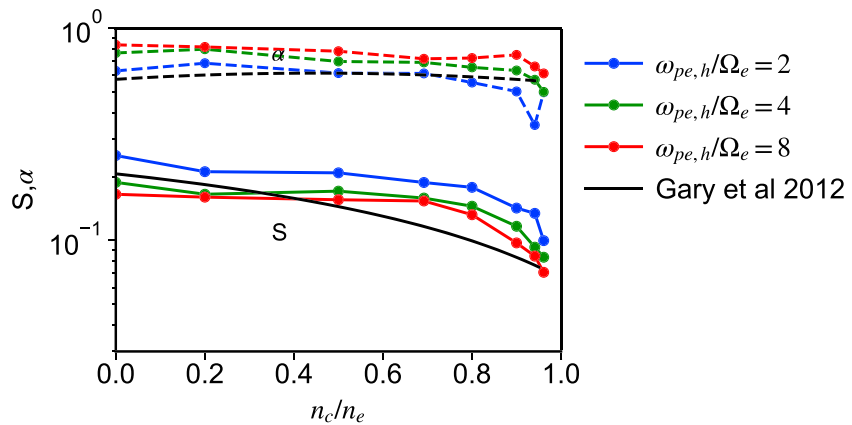
Figure 3. This figure shows how fitting parameters, S and α, change with cold electron proportion. Different colors represent different hot electron density, dashed lines for α and solid lines for S. The results obtained from linear analysis (Gary et al., 2012) are shown as black lines.

are shown in Figure 2. For saturation $\beta_\| \leq 2.5$, which is the range of $\beta_\|$ considered by Gary et al. (2012), A and $\beta_\|$ satisfy the inverse relation predicted by the linear theory. However, for all $\beta_\|$ considered, we note that as $\omega_{pe,c}/\Omega_e$ increases, the A-$\beta_\|$ relation deviates from the inverse relation $A = S/\beta_\|^\alpha$. For example, for $\omega_{pe,c}/\Omega_e = 20$, saturation A increases with saturation $\beta_\|$ for $\beta_\| \gtrsim 2$.
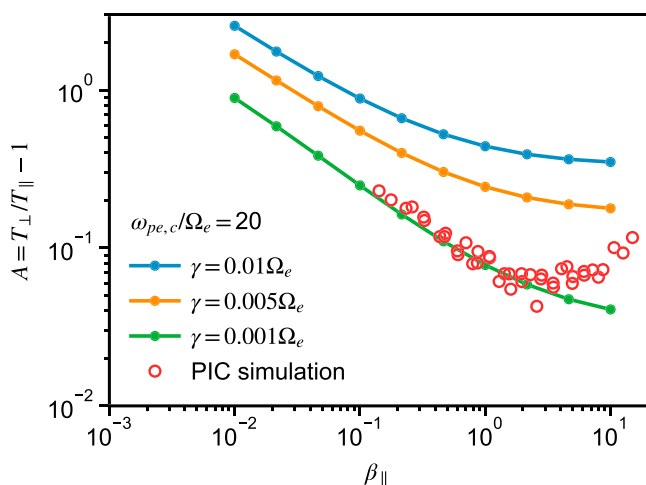
To better describe the A-$\beta_\|$ relation for a larger range of $\beta_\|$, we use $A = S_1/\beta_\|^{\alpha_1} + S_2\beta_\|^{\alpha_2}$ to fit A and $\beta_\|$, where S_1, S_2, α_1, and α_2 are all nonnegative. This fitting function has the property that as $\beta_\| \to 0$, the first term dominates, consistent with previous results. The fitting results are shown in Figure 2 for the four characteristic cases presented. It is clear that a critical value of $\beta_\|$, $\beta_{\lim}$, separates A and $\beta_\|$ relation into two regions. Results with $\beta_\| < \beta_{\lim}$ follows the well-known inverse relation $A = S/\beta_\|^\alpha$, while for $\beta_\| > \beta_{\lim}$, A and $\beta_\|$ are positively correlated at saturation. In addition, the value of $\beta_{\lim}$ decreases with increasing n_c/n.

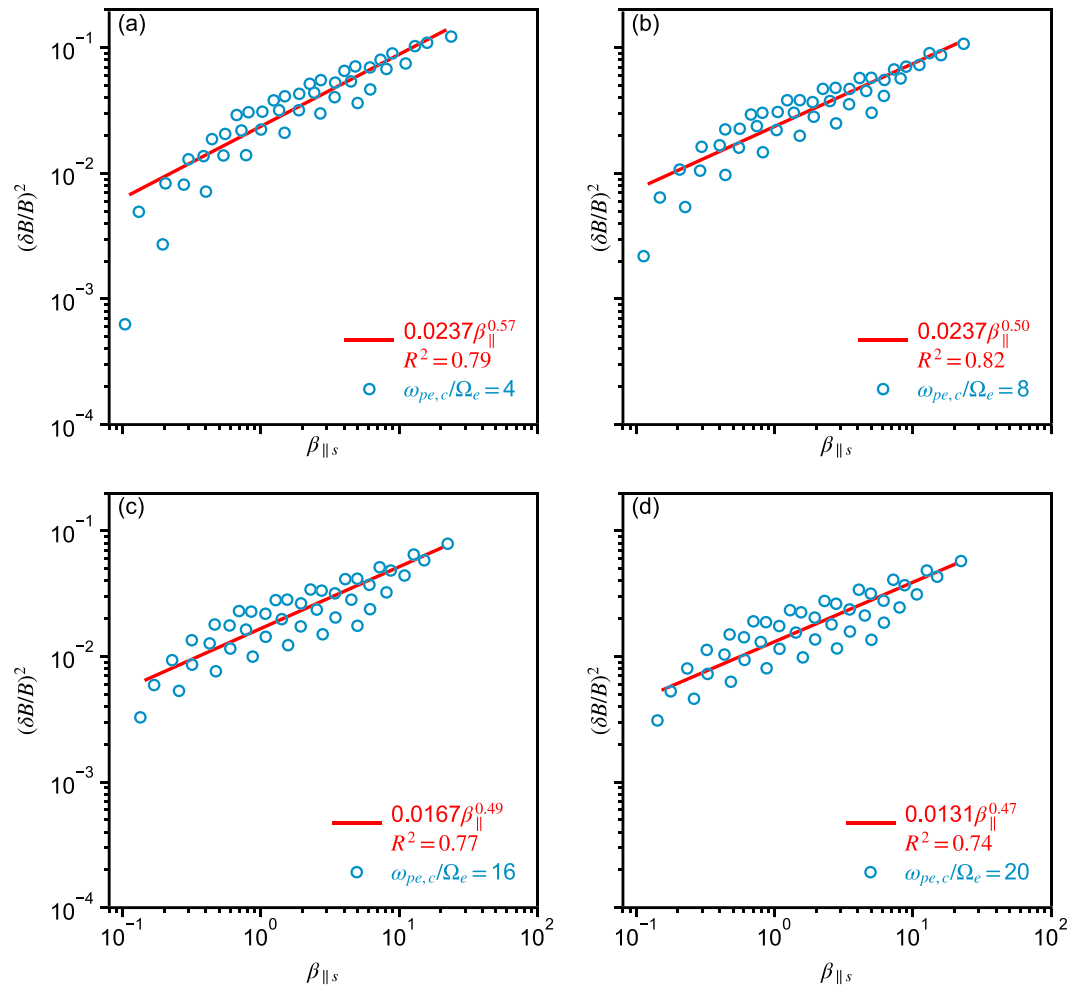### 4.2. Comparison of the A-$\beta_\|$ Relation With Linear Theory
In this section, we compare the PIC simulation results with linear theory as described by Gary et al. (2012). First, we limit $\beta_\|$ to be in the same range as that considered by Gary et al. (2012), $\beta_\| < 2.5$, and performs linear fitting between $\log A$ and $\log \beta_\|$ to obtain S and α, as shown in Figure 2. We also perform two more batches of simulations with different $\omega_{pe,h}/\Omega_e$'s, 2 and 8, to see if there is any dependence on $\omega_{pe,h}/\Omega_e$ of S and α.

The dependencies of S and α for $\beta_\| < 2.5$ on n_c/n and $\omega_{pe,h}/\Omega_e$ are shown in Figure 3. The results of linear analysis with $\gamma_{\max} = 0.001\Omega_e$ (Gary et al., 2012), equations (2) and (3) are presented as black solid lines. It is seen that PIC simulation results show the same trend of variation of $S(n_c/n)$ and $\alpha(n_c/n)$ as linear theory predictions, and the difference between simulation and linear theory values of S and α is within a factor of $2 \sim 3$. This suggests that for $\beta_\| < 2.5$, our simulation results agree quite well with previous linear analysis (Gary et al., 2012). Figure 3 also show that values of S and α vary by less than a factor of 2 when $\omega_{pe,h}/\Omega_e$ changes from 2 to 8.

Figure 4. A and $\beta_\|$ relation obtained from different methods. Three groups of lines in different colors represent results from linear analysis, while blue, orange, and green lines stand for $\gamma_{\max}/\Omega_e$ equals 0.01, 0.005, and 0.001, respectively. The red circles mark the results of particle-in-cell (PIC) simulation at saturation.

Now we remove the limitation of $\beta_\|$ and see if linear theory show similar qualitative change in the A-$\beta_\|$ relation if $\beta_\|$ becomes large for higher n_c/n. We follow the method of Gary et al. (2012), with $\omega_{pe,h}/\Omega_e = 4$ and $\omega_{pe,c}/\Omega_e = 20$. We show linear theory calculations with three different $\gamma_{\max}$: $0.01\Omega_e$, $0.005\Omega_e$, and $0.001\Omega_e$. Both linear theory and PIC simulation results are shown in Figure 4. It is clear from this figure that, even though linear theory results show some deviations from $A = S/\beta_\|^\alpha$ as $\beta_\|$ increases beyond 2.5, there is no qualitative change in the dependence for the range of $\beta_\|$ considered. On the other hand, the PIC simulation results show that as $\beta_\|$ increases, A first decreases and then increases with

Figure 5. The circles mark saturated wave magnetic field intensity (regulated as $(\delta B/B)^2$) and $\beta_\parallel$. And the red line shows the least absolute deviation fitting result. Panels (a to d) show situations with $\omega_{pe,c}/\Omega_e = 4, 8, 16$, and 20, respectively.

increasing $\beta_\parallel$. This kind of change is not described by linear theory and suggests the importance of using a self-consistent approach to obtain the A-$\beta_\parallel$ relation.

4.3. The Dependence of Wave Amplitude on Plasma Parameters

In this section, we investigate the dependence of saturation wave intensity on $\beta_\parallel$ at saturation and initial maximum linear growth rate with the a cold electron component.

An et al. (2017) used 2-D PIC simulations to obtain relation between wave intensity $(\delta B/B)^2$ with $\beta_\parallel$ at saturation with a single hot electron component. They found that saturated wave intensity $(\delta B/B)^2$ roughly scales with $\beta_\parallel$ as $\beta_\parallel^\theta$ with $\theta = 1.2 \sim 2$. Our results with only a hot electron component (Figure 1) show that $(\delta B/B)^2 \propto \beta_\parallel^{0.73}$. The difference in the θ index between our results with those of An et al. (2017) is caused by the different ranges of $\beta_\parallel$. In our results, $\beta_\parallel$ is in the range of $[0.1, 20]$, while that in An et al. (2017) is in the range of $[10^{-2}, 3]$. If we only consider simulations with $0.1 < \beta_\parallel < 3$, our results are consistent with those of An et al. (2017). For example, from An et al. (2017), we can see $(\delta B/B)^2$ is roughly 10^{-3} when $\beta_\parallel = 0.1$, and about 10^{-2} when $\beta_\parallel = 1$. These values are quite close to our simulation results in Figure 1b. Note that our results are more consistent with those of Tao et al. (2017), who used quasi-linear analysis to obtain the dependence of $(\delta B/B)^2$ on $\beta_\parallel$, because both studies have similar ranges of $\beta_\parallel$.

Now we present the dependence of $(\delta B/B)^2$ on $\beta_\parallel$ at saturation and the maximum initial linear growth rate with a cold electron component. We show simulation results with $\omega_{pe,c}/\Omega_e = 4, 8, 16, 20$, and $\omega_{pe,h}/\Omega_e = 4$ in Figures 5 and 6. From Figure 5, $(\delta B/B)^2$ scales with $\beta_\parallel$ roughly as $\beta_\parallel^\theta$ with $0.45 < \theta < 0.75$ for the range of $\beta_\parallel$
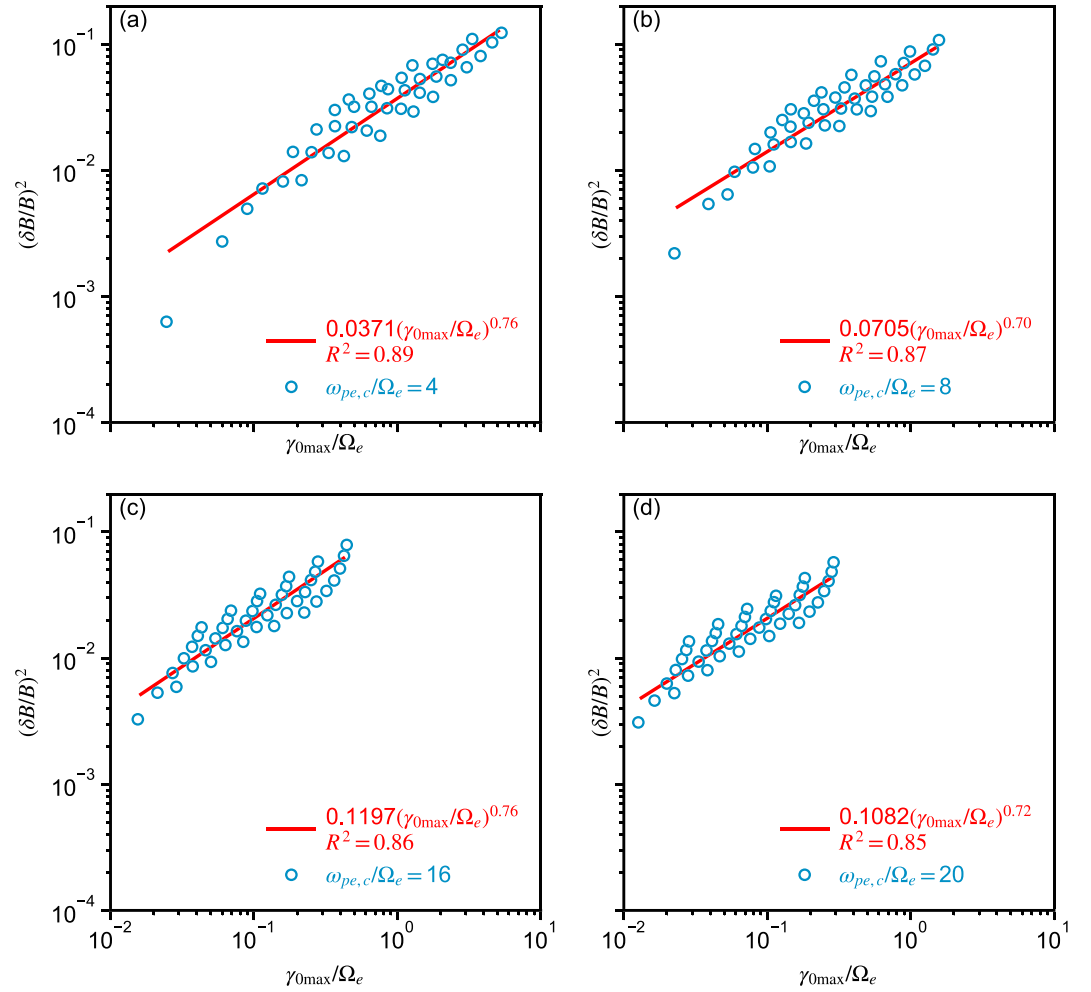
Figure 6. The circles mark saturated wave magnetic field intensity $(\delta B/B)^2$ and initial maximum linear growth rate γ_{max}. And the red line shows the least absolute deviation fitting result. Panels (a to d) shows situations with $\omega_{pe,c}/\Omega_e = 4, 8, 16,$ and 20, respectively. Note that the proportion of cold electron strongly affects linear growth rate, so the γ_{max}'s have different ranges in the four panels.

considered. As the percentage of cold electrons (n_c/n) is increased, $(\delta B/B)^2$ still scales with $\beta_\parallel$, but the slope decreases slightly with increasing n_c/n. As $\omega_{pe,c}/\Omega_e$ increases from 2 to 20, θ decreases from 0.57 to 0.47. Figure 6 shows the dependence of $(\delta B/B)^2$ on the maximum initial linear growth rate γ_{max}. Consistent with Tao et al. (2017), we find $(\delta B/B)^2$ scales better with γ_{max} than $\beta_\parallel$ according to the value of the R^2 parameter. The dependence of $(\delta B/B)^2$ on γ_{max} can be roughly written as $(\delta B/B)^2 \propto \gamma_{max}^\mu$, where the slope μ varies between 0.70 and 0.76 (Figure 6). This value is close to the quasi-linear theory results obtained by Tao et al. (2017), who showed that $(\delta B/B)^2 = 0.17\gamma_{max}^{0.76}$ with only hot electrons.

5. Conclusions

In this work, we have used self-consistent PIC simulations to investigate the saturation properties of whistler waves in a uniform background magnetic field with both cold and hot electrons. Our main conclusions can be summarized as follows.

1, We confirm previous linear theory of Gary et al. (2012) that in a plasma with a cold electron component, A and $\beta_\parallel$ roughly satisfy $A = S/\beta_\parallel^\theta$ at saturation when $\beta_\parallel < 2.5$. This agrees also with previous results given by linear theory (Gary & Wang, 1996) and quasi-linear theory (Kim et al., 2017; Tao et al., 2017) for a plasma without cold electrons. The dependence of S and α on n_c/n also agrees with predictions of Gary et al. (2012). We also investigate the effect of hot electron density by using $\omega_{pe,h}/\Omega_e = 2, 4, 8$. We find that for the values of $\omega_{pe,h}/\Omega_e$ considered, S and α change within about a factor of 2 for the range of $\omega_{pe,h}/\Omega_e$ considered.

2, In more general cases where $\beta_\parallel$ can be larger than 2.5, we showed that the inverse relation between A and $\beta_\parallel$ does not necessarily hold, especially when $\omega_{pe,c}/\Omega_e$ is large. So we proposed a new function, $A = S_1/\beta_\parallel^{\alpha_1} + S_2\beta_\parallel^{\alpha_2}$, with both S and α being positive, to take into account the increase of A with increasing $\beta_\parallel$ at large $\beta_\parallel$. We also demonstrated that linear theory cannot predict this kind of A-$\beta_\parallel$ relation. This implies the importance of using self-consistent approaches to understand the A-$\beta_\parallel$ relation.

3, We investigated the dependence of the saturation wave intensity as a function of saturation $\beta_\parallel$ and maximum initial linear growth rate. We found that with the presence of cold electrons, the scaling index θ in $(\delta B/B)^2 \propto \beta_\parallel^\theta$ decreases from 0.73 to 0.47 as $\omega_{pe,c}/\Omega_e$ increases from 2 to 20. On the other hand, the scaling index μ as in $(\delta B/B)^2 \propto \gamma_{\max}^\mu$ changes between 0.70 and 0.76. The R^2 parameter suggests that it is better using $\gamma_{\max}$ than $\beta_\parallel$ to model saturation wave intensity.

The scaling laws obtained from our simulations between saturation properties of waves and the initial conditions show the potential of incorporating microscopic wave excitation and saturation processes in global macroscopic models. However, our simulations assume an infinite uniform plasma and therefore the periodic boundary conditions, while in Earth's magnetosphere, open boundary conditions for waves and a dipole background magnetic field might be more appropriate. Taking more realistic boundary and plasma configuration conditions into consideration is beyond the scope of this work and will be left as a future study.

References

An, X., Yue, C., Bortnik, J., Decyk, V., Li, W., & Thorne, R. M. (2017). On the parameter dependence of the whistler anisotropy instability. *Journal of Geophysical Research: Space Physics*, *122*, 2001–2009. https://doi.org/10.1002/2017JA023895

Davidson, R. C., Hammer, D. A., Haber, I., & Wagner, C. E. (1972). Nonlinear development of electromagnetic instabilities in anisotropic plasmas. *The Physics of Fluids*, *15*(2), 317–333.

Gary, S. P., Lavraud, B., Thomsen, M. F., Lefebvre, B., & Schwartz, S. J. (2005). Electron anisotropy constraint in the magnetosheath: Cluster observations. *Geophysical Research Letters*, *32*, L13109. https://doi.org/0.1029/2005GL023234

Gary, S. P., Liu, K., Denton, R. E., & Wu, S. (2012). Whistler anisotropy instability with a cold electron component: Linear theory. *Journal of Geophysical Research*, *117*, A07203. https://doi.org/10.1029/2012JA017631

Gary, S. P., Liu, K., & Winske, D. (2011). Whistler anisotropy instability at low electron β: Particle-in-cell simulations. *Physics of Plasmas*, *18*(8), 082902. https://doi.org/10.1063/1.3610378

Gary, S. P., & Wang, J. (1996). Whistler instability: Electron anisotropy upper bound. *Journal of Geophysical Research*, *101*(A5), 10,749–10,754.

Horne, R. B., Thorne, R. M., Shprits, Y. Y., Meredith, N. P., Glauert, S. A., Smith, A. J., & Decreau, P. M. E. (2005). Wave acceleration of electrons in the Van Allen radiation belts. *Nature*, *437*, 227–230. https://doi.org/10.1038/nature03939

Jordanova, V. K., Thorne, R. M., Li, W., & Miyoshi, Y. (2010). Excitation of whistler mode chorus from global ring current simulations. *Journal of Geophysical Research*, *115*, A00F10. https://doi.org/10.1029/2009JA014810

Kim, H. P., Hwang, J., Seough, J. J., & Yoon, P. H. (2017). Electron temperature anisotropy regulation by whistler instability. *Journal of Geophysical Research: Space Physics*, *122*, 4410–4419. https://doi.org/10.1002/2016JA023558

Nishimura, Y., Bortnik, J., Li, W., Thorne, R. M., Lyons, L. R., Angelopoulos, V., & Auster, U. (2010). Identifying the driver of pulsating aurora. *Science*, *330*, 81–84. https://doi.org/10.1126/science.1193130

Reeves, G. D., Spence, H. E., Henderson, M. G., Morley, S. K., Friedel, R. H. W., Funsten, H. O., & Niehof, J. T. (2013). Electron acceleration in the heart of the Van Allen radiation belts. *Science*, *341*, 991–994. https://doi.org/10.1126/science.1237743

Tao, X. (2014). A numerical study of chorus generation and the related variation of wave intensity using the DAWN code. *Journal of Geophysical Research: Space Physics*, *119*, 3362–3372. https://doi.org/10.1002/2014JA019820

Tao, X., Chen, L., Liu, X., Lu, Q., & Wang, S. (2017). Quasilinear analysis of saturation properties of broadband whistler mode waves. *Geophysical Research Letters*, *44*, 8122–8129. https://doi.org/10.1002/2017GL074881

Thorne, R. M., Li, W., Ni, B., Ma, Q., Bortnik, J., Chen, L., & Kanekal, S. G. (2013). Rapid local acceleration of relativistic radiation-belt electrons by magnetospheric chorus. *Nature*, *504*, 411–414. https://doi.org/10.1038/nature12889

Thorne, R. M., Ni, B., Tao, X., Horne, R. B., & Meredith, N. P. (2010). Scattering by chorus waves as the dominant cause of diffuse auroral precipitation. *Nature*, *467*, 943–946. https://doi.org/10.1038/nature09467

Xiao, F., Zhou, Q., Zheng, H., & Wang, S. (2006). Whistler instability threshold condition of energetic electrons by kappa distribution in space plasmas. *Journal of Geophysical Research*, *111*, A08208. https://doi.org/10.1029/2006JA011612

Yue, C., An, X., Bortnik, J., Ma, Q., Li, W., Thorne, R. M., & Kletzing, C. A. (2016). The relationship between the macroscopic state of electrons and the properties of chorus waves observed by the Van Allen probes. *Geophysical Research Letters*, *43*, 7804–7812. https://doi.org/10.1002/2016GL070084